Investigation of Early Events in FcεRI-Mediated Signaling using a Detailed Mathematical Model[1]

James R. Faeder,[1] William S. Hlavacek,[*] Ilona Reischl,[2] Michael L. Blinov,[*] Henry Metzger,[3] Antonio Redondo,[4] Carla Wofsy,[*¶] and Byron Goldstein[2*]

Running Title: Mathematical Modeling of FcεRI Signaling

Keywords: signal transduction, FcεRI, mast cells/basophils, Lyn, Syk, mathematical modeling

Draft: 11/26/2002

[1] Theoretical Biology and Biophysics Group, Theoretical Division, Los Alamos National Laboratory, Los Alamos, NM 87545

[2] US Food and Drug Administration, Center for Biologics Evaluation and Research, National Institutes of Health, Bethesda, MD 20892

[3] Arthritis and Rheumatism Branch, National Institute of Arthritis and Musculoskeletal and Skin Diseases, National Institutes of Health, Bethesda, MD 20892

[4] Theoretical Chemistry and Molecular Physics Group, Theoretical Division, Los Alamos National Laboratory, Los Alamos, NM 87545

[¶] Department of Mathematics and Statistics, University of New Mexico, Albuquerque, NM 87131

Abstract

Aggregation of FcεRI on mast cells and basophils leads to autophosphorylation and increased activity of the cytosolic protein tyrosine kinase Syk. We investigate the roles of the Src kinase Lyn, the ITAMs (immunoreceptor tyrosine-based activation motifs) on the β and γ subunits of FcεRI, and Syk itself in the activation of Syk. Our approach is to build a detailed mathematical model of reactions involving FcεRI, Lyn, Syk, and a bivalent ligand that aggregates FcεRI. We apply the model to experiments in which covalently cross-linked IgE dimers stimulate rat basophilic leukemia (RBL) cells. The model makes it possible to test the consistency of mechanistic assumptions with data that, alone, provide limited mechanistic insight. For example, the model helps sort out mechanisms that jointly control dephosphorylation of receptor subunits. In addition, interpreted in the context of the model, experimentally observed differences between the β and γ chains with respect to levels of phosphorylation and rates of dephosphorylation indicate that most cellular Syk, but only a small fraction of Lyn, is available to interact with receptors. We also show that although the β ITAM acts to amplify signaling in experimental systems where its role has been investigated, there are conditions under which the β ITAM will act as an inhibitor.

Introduction

There is increasing recognition that mathematical modeling can be a valuable interpretive and predictive tool for understanding cell signaling cascades (1, 2). In the case of the signaling cascade initiated by the aggregation of FcεRI, the high affinity receptor for IgE, detailed molecular-level models have been used to characterize the role of Lyn kinase in the initiation and regulation of FcεRI tyrosine phosphorylation (3, 4). We have recently extended these earlier models to investigate the separate roles of the receptor subunits and the kinases Lyn and Syk in the phosphorylation and activation of Syk (5). Here we provide a detailed description of the model and improved estimates of parameters based on direct experimental measurements and comparison of model predictions with both new and previously reported experimental data.

FcεRI is a member of the family of multichain immune recognition receptors (MIRR), which also includes the B cell receptor (BCR) and T cell receptor (TCR) (6). The subunits of the MIRR can be divided into those that participate in binding and those that participate in signaling. All of the signaling subunits, but none of the binding subunits, have at least one copy of a common sequence in their cytoplasmic domains called an ITAM (immunoreceptor tyrosine-based activation motif) (7, 8). The earliest cellular response in MIRR-mediated signal transduction is the phosphorylation of ITAM tyrosines by Src family protein tyrosine kinases (PTKs). A member of a second PTK family—Syk in the case of FcεRI and the BCR, and predominantly Zap70 in the case of the TCR—can then bind to doubly phosphorylated ITAMs, become phosphorylated, and mediate additional signaling events.

We model the tetrameric form of FcεRI, which has an α chain that binds IgE and three ITAM-containing subunits, a β chain and two disulfide-linked γ chains. The tetrameric receptor is the only form found in rodent cells and is also expressed on human basophils and mast cells (9). Human basophils and mast cells also express a trimeric form of the receptor that is missing the β subunit, and other human cell types express only the trimeric form (9).

The unphosphorylated β chain associates weakly with the Src family kinase Lyn, which is anchored to the inner layer of the plasma membrane (10-14). Upon receptor

aggregation, Lyn transphosphorylates tyrosines in the β and γ ITAMs (15, 16). There is a much stronger association of Lyn through its SH2 domain with the phosphorylated β ITAM (11, 15). The cytosolic PTK Syk binds with high affinity, through its two SH2 domains, to the doubly phosphorylated γ ITAM (17, 18). Syk is phosphorylated on multiple tyrosines by both Lyn and Syk (19-22), with Syk playing the major role in phosphorylating the two tyrosines, 519 and 520, in the Syk activation loop (23, 24). This yields a fully activated Syk that is required for calcium mobilization (22-24).

The model that we present describes association, dissociation, and phosphorylation reactions among four components: the receptor FcεRI, a bivalent ligand that aggregates receptors into dimers, and the PTKs Lyn and Syk. The model also includes dephosphorylation reactions mediated by a pool of protein tyrosine phosphatases. Even with simplifying assumptions, justified below based on experimental considerations, the reactions among the components generate a network of 354 distinct molecular species. The model predicts levels of association and phosphorylation of molecular complexes as they vary with time, ligand concentration, concentrations of signaling components, or genetic modifications of the interacting proteins. Therefore the model can be used to analyze a wide variety of experimental data and the data provide multiple tests of the model. We estimate parameters for rat basophilic leukemia (RBL) cells stimulated by covalently cross-linked IgE dimers (25-27).

The model survives a stringent test. For experiments that carry information relevant to the experimental system we consider, and that are expected to reflect only the molecules in the model, we identify a set of reaction rate constants for which model predictions are consistent, quantitatively, with published data and with additional experiments that we report here.

The analysis we present offers new information about the factors that control receptor dephosphorylation, access of receptors to Lyn and Syk, and the role of the phosphorylated β ITAM. We find that intrinsic rates of ITAM dephosphorylation are orders of magnitude faster than the apparent rates measured experimentally. SH2 domains bound to phosphotyrosines protect the sites they are bound to from dephosphorylation (28). Because SH2-bound Lyn and Syk protect phosphorylated sites from dephosphorylation, observed time courses of ITAM dephosphorylation reflect,

along with intrinsic phosphatase activity, the amounts of Lyn and Syk available to bind, through their SH2 domains, to phosphorylated ITAMs, and the rate constants for binding and dissociation. The amount of phosphorylation of the γ ITAM relative to that of β is another important point of contact between model and experiment, where model predictions differ sharply depending on the amount of Syk available to interact with FcεRI. For the model to be consistent with data, much more Syk than Lyn must be available. The model also shows that the β ITAM may act as a strong or weak amplifier of signaling, or even as a weak inhibitor, depending on the rate at which Lyn transphosphorylates the γ ITAM. Parameter estimates presented here reflect experimental evidence that the β ITAM functions as an amplifier (29).

Materials and Methods

Cell lysates and immunoprecipitation.

RBL-2H3 cells were harvested with trypsin-EDTA, washed in buffer A (150 mM NaCl, 5 mM KCl, 5.4 mM glucose, 1.8 mM $CaCl_2$, 1 mM $MgCl_2$, 25 mM Pipes, pH 7.2 containing 0.1 % BSA) and re-suspended in buffer A at 1.5×10^7 cells/ml. Cells were reacted with different doses of either monomeric or chemically cross-linked dimers of mouse IgE (27) for 10 min, prior to cell lysis in 0.5 volumes of ice-cold 3x solubilization buffer (pH 7.6) to yield a final concentration of 0.17% TX-100, 50 mM Tris, 50 mM NaCl, 5 mM EDTA, 1 mM Na_3VO_4, 5 mM $Na_4P_2O_7$, 50 mM NaF, 2 mM iodoacetate, 1 mM phenylmethanesulfonyl-fluoride, 10 μg/ml each of aprotinin, leupeptin and pepstatin A, and agitated for 30 min at 4^oC. After 5 min of centrifugation, target proteins were immunoprecipitated from the supernatant with shaking for 3 h at 4^oC. IgE-bound FcεRI was precipitated with goat anti-mouse IgE antibodies (ICN Biomedicals, Inc., Aurora, OH) using protein A Sepharose beads (Amersham Biosciences, Piscataway, NJ). Phosphorylated proteins were precipitated with mAb 4G10 (Upstate Biotechnologies, Lake Placid, NY) using protein G Sepharose beads (Amersham Biosciences, Piscataway, NJ). Syk was precipitated using the scFv G4G11 (30) pre-bound overnight to anti-myc beads (clone 9E10, Covance, Richmond, CA).

Western blot

Samples were run on 8% or 12% Tris-Glycine Gels (Invitrogen, Carlsbad, CA) followed by semi-dry transfer to Protran® nitrocellulose membranes (Schleicher & Schuell, Dassel, Germany). Following a blocking step (31, 32), phosphorylated proteins were detected with 4G10-biotin (Upstate Biotechnologies) and NeutrAvidin[TM]-HRP (Pierce, Rockford, IL). The FcεRI β-chain was detected with antibody JRK (33) and Syk with a monoclonal anti-Syk , both followed by HRP-conjugated sheep-anti-mouse F(ab)$_2$ (Sigma Immunochemicals, St. Louis, MO), ECL[TM] and exposure of Hyperfilm[TM] ECL[TM] (both from Amersham). Stripping of membranes was performed with Restore[TM] Western Blot Stripping buffer (Pierce) for 15 min at room temperature, followed by two 10-min washes in TTBS (50 mM Tris, 150 mM NaCl, 0.05% (v/v) Tween-20, adjusted to pH 7.5 with HCl).

Quantification of Syk protein

Syk SH2-GST fusion protein was produced and purified as described (34) and used to generate a calibration curve. The construct, with 492 residues total, consists of a 24 amino acid leader sequence, residues 10 to 261 from human Syk and GST from *Schistosoma japonicum*, has a molecular weight of 56.4 kDa, and a molar extinction coefficient of 78489 cm^{-1}M^{-1} (35). A stock solution (O.D. of 0.09) was diluted in siliconized tubes in buffer A (150 mM NaCl, 5 mM KCl, 25 mM Pipes, 5.4 mM glucose, 1 mM MgCl$_2$, 1.8 mM CaCl$_2$, 0.1% BSA, adjusted to pH 7.2) and run on the same gel either separately or mixed with lysate of RBL cells. The relative amounts of the construct and the endogenous protein were determined by quantitating the amount of bound anti-Syk antibody, directed against the SH2 domains of Syk (36), by densitometric evaluation of Western blots. The average number of Syk molecules per RBL cell based on 15 measurements from four experiments was calculated from the calibration curve.

Mathematical Model

The model is based on the following sequence of early events in signaling through the FcεRI receptor (37, 38): ligand-receptor binding leading to aggregation of receptors at the plasma membrane, transphosphorylation of specific tyrosine residues in the ITAMs

of aggregated receptors by constitutively associated Lyn kinase, recruitment of additional Lyn and of Syk kinase to the phosphorylated ITAMs, and subsequent transphosphorylation of Syk by both Lyn and Syk. The full activation of Syk through the phosphorylation of two adjacent tyrosine residues in the activation loop of its kinase domain is required for downstream events including calcium mobilization and degranulation (23). Although these events are typically described as a linear sequence of chemical reactions, the early signaling events form a highly branched chemical network involving a large number of different chemical species.

The model was constructed in the following steps, which can serve as a general template for the development of signaling models: 1) Identify components and their interactions to generate a set of feasible chemical species that participate in the signaling process being studied, 2) develop reaction rules for these species, to construct a chemical network, 3) determine values of reaction rate constants and initial concentrations based on direct measurements and other experimental observations, 4) convert the network into a predictive mathematical model consisting of a set of coupled differential equations, 5) solve the equations numerically to obtain predictions for a given set of initial conditions, 6) modify the values of specific parameters as necessary to improve agreement between the predictions of the model and experimental observations. Although our model is specific to FcεRI-mediated signaling, it can be adapted to other signaling pathways that share a similar sequence of initial events, e.g. B-cell receptor signaling, and it can be extended to include additional signaling molecules, such as co-receptors, specific phosphatases, and solution and surface-associated adapters.

Components

The tetrameric FcεRI is modeled as three subunits, with the disulfide-bonded pair of γ chains treated as one unit (Fig. 1a). The extracellular region of the α chain binds to the Fc portion of IgE. The ligand shown here is a covalently cross-linked dimer of IgE (25), which can induce receptor phosphorylation and degranulation of RBL cells and is convenient because it forms only dimer receptor aggregates and its kinetics have been well-characterized (27). The model can be applied, however, to any situation where the ligand is bivalent and the receptor is effectively monovalent, as would be the case if

bispecific IgE were used to sensitize the cells (39). In this case the high-affinity IgE molecule would be considered part of the binding subunit of the receptor.

The β subunit and the γ dimer contain the ITAMs that, upon phosphorylation, become binding sites for the SH2 domains of the two kinases, Lyn and Syk. The major simplification we make in the model is that multiple tyrosine residues on receptor subunits and Syk are treated as single units of phosphorylation, as indicated in Fig. 1. For example, the β ITAM contains three tyrosines, but in the model the ITAM is either phosphorylated or not phosphorylated. Sites of Syk tyrosine phosphorylation are lumped into two units: the activation loop, which is phosphorylated by Syk, and the linker region, which is phosphorylated by Lyn.

Figure 1b shows the states of the β chain and γ dimer included in the model. Each unit can be phosphorylated or unphosphorylated, and can be associated with a kinase in any of several states. In the model, each β chain and γ dimer can bind only a single kinase molecule at a time. The actual stoichiometry of Syk binding to the γ dimer is unknown. The assumption that only one Syk binds to a γ dimer seems reasonable given the size disparity between the γ chain (9 kD) and Syk (72 kD). Modifying the model to allow two Syk molecules to bind to the two chains in a γ dimer would increase the complexity of the model, but such complexity can be accommodated if the stoichiometry is determined to be two.

The model permits a large number of receptor states (Fig. 1b,c). Since the state of each subunit is independent of the states of the other subunits, the total number of monomer states is $n_\alpha n_\beta n_\gamma = 48$. In a dimer, each α subunit must be engaged with the ligand, so the total number of dimer states is $n_\beta n_\gamma (n_\beta n_\gamma + 1)/2 = 300$. In addition, there are six non-receptor states—free ligand, free Lyn, and Syk in each of its four possible states of phosphorylation—to give a total of 354 distinct chemical species in the model.

Reaction classes

The signaling model is composed of the 354 chemical species we have just described and the chemical reactions that connect them. The reaction network is constructed using a set of reaction rules or classes, each of which describes the formation

and breaking of a chemical interaction based only on the presence of specific motifs in the chemical species involved. For example, as illustrated in Fig. 2, there are only two classes of reaction to describe the formation of a ligand-receptor bond, depending only on whether one Fc region of the IgE dimer is already bound to receptor. There is experimental evidence that the ligand-receptor interactions in this system are unaffected by modifications of the cytoplasmic portion of the receptor (32). Therefore we assume that rate constants for binding reactions are independent of the states of β and γ subunits. As a result, only two rate constants parameterize the 48 reactions (considering forward and reverse reactions separately) for the binding of free IgE dimer to FcεRI. Similarly, only two rate constants parameterize the far greater number of aggregation reactions (1152), where a free receptor binds to an IgE dimer that is already bound to a receptor. In the current model, 15 reaction classes and 21 rate constants are used to describe the 3680 chemical transformations that can occur. In this way the limited experimental information about the kinetics of signaling reactions can be combined with the much larger amount of information about the structure of the components and the interactions among them.

Each reaction class is represented in Fig. 2 by its simplest member, i.e., the reactants shown have the minimal set of modifications required to carry out the given reaction. The full list of 3680 possible reactions is generated by a computer algorithm that, for each reaction class, checks each of the chemical species to see if it can participate in a reaction in that class. For example, a dimer with no associated Lyn or Syk cannot participate in a phosphorylation reaction but can participate in some other classes of reactions, for example the constitutive association of Lyn. The rate of each reaction is simply the product of the rate constant and each of the reactant concentrations (elementary reaction kinetics). The rate of change of each species involved in a reaction is increased by this rate for product species and decreased by this rate for reactant species.

Network structure and parameters

We will now describe the reaction events and associated parameters in more detail. The reaction model requires as input not only the rate constants associated with

each of the reactions but also the initial concentrations of each of the components, which are specific to the cell type being modeled. In this work we have chosen parameters appropriate to the RBL cell in order to facilitate comparison between the simulation results and experiments. A summary of the parameters is given in Table 1.

The reactions that describe ligand-receptor binding and ligand-induced receptor aggregation have been used previously to model the binding kinetics of the ^{125}I-labeled IgE dimers to RBL cells (27). The four rate constants determined by a fit to the experimental data in that work are given in Table 1. We have set the reverse rate constants to zero in the simulations, which has a negligible effect on time scales under a few hours, but facilitates checking the numerical results for convergence. We estimate that there are about 4×10^5 FcεRI per cell for the RBL cells used in the current study.

The model permits Lyn to associate with the receptor in two ways. Lyn associates weakly with the unphosphorylated receptor (10-12) through an interaction between its unique domain and the C-terminal cytoplasmic tail of the β subunit (13, 14). This association is denoted in Fig. 2 as "constitutive Lyn binding." Upon phosphorylation of the β ITAM, Lyn is recruited with much higher affinity through its SH2 domain (11, 15, 40). These reactions and their associated parameters are based on our earlier model of Lyn activity that did not include Syk (3). The amount of Lyn available to bind receptors was fit to receptor phosphorylation kinetics and determined to be about 7% of the number of FcεRI (3). Although this number is far lower than the actual number of Lyn molecules typically measured in RBL cells, several competition experiments (41, 42) have demonstrated that Lyn kinase is available in limiting concentrations in RBL cells. The equilibrium constant for the constitutive interaction was based on the results of chemical cross-linking experiments that indicated about 3–4% of receptors in resting RBL cells were associated with Lyn (11). Finally, the equilibrium constant for the high affinity interaction was estimated from equilibrium constants of similar SH2-phosphopeptide interactions measured in solution (3). The four rate constants for Lyn association are determined by the two equilibrium constants, the assumption that the forward rate constant is identical for both forms of association, and a fit of the model to β ITAM dephosphorylation data, as described below. As a result of this fitting, we estimate that the rate constant for dissociation of Lyn from the

phosphorylated ITAM, k^*_{-L}, is about an order of magnitude faster than previously estimated (3).

Syk associates with FcεRI primarily through an interaction between its tandem SH2 domains and the doubly phosphorylated γ ITAM (34, 40, 43, 44). Syk has at least a 1000-fold lower affinity for the singly phosphorylated γ ITAM peptide (34) and at least a 20-fold lower affinity for the doubly phosphorylated β ITAM (44). The equilibrium dissociation constant, K_d, for the interaction of Syk's tandem SH2 domains with the diphosphorylated γ ITAM peptide sequence has been determined both with surface plasmon resonance (44) and with a scintillation proximity assay (34) at 25°C and comparable results were obtained. We use a value of 2.6 nM for K_d in the current model. The only two measured values for the dissociation of Syk's tandem SH2 domains from a diphosphorylated ITAM peptide are 0.01 s^{-1} (34) and 0.7 s^{-1} (45) at 25°C. In addition, Grucza et al. have observed a very strong temperature dependence of binding in the range 25–37°C which they attributed to a conformational change in Syk (45). The dissociation rate constant in our model is obtained from a fit of model predictions to the observed rate of γ ITAM dephosphorylation, as described below, and is intermediate between the measured values. It is also very similar to the rate constant we estimate for Lyn dissociation from the phosphorylated β ITAM. In the current parameter set, the Syk dissociation rate constant does not change when Syk is phosphorylated (20, 21), although the structure of the model permits such a distinction if subsequent evidence shows that this regulatory mechanism is important in FcεRI-mediated pathways. We estimate that about 3.4×10^5 Syk molecules per cell are present in the RBL cells used in the current study. In contrast with the case of Lyn kinase, the analysis presented below indicates that all or most of the Syk is available to interact with receptors.

Lyn associated with a receptor aggregate can transphosphorylate both the β and γ ITAMs (15) and Syk associated with an adjacent receptor (19, 21). As in our previous model of FcεRI-mediated Lyn activity (3), it is assumed that all the available Lyn is in a form that, when associated with an aggregated receptor, can initiate transphosphorylation. We do not address the issues of how the size of the pool of available Lyn or the activity of Lyn is regulated. The model is consistent with the finding that a single Lyn molecule

in an aggregate is sufficient to induce receptor phosphorylation (4), which demonstrates that Lyn clustering and Lyn-Lyn transphosphorylation within receptor aggregates are not required for Lyn activity. In general, the results of the model are not sensitive to the absolute rates of phosphorylation, which are chosen simply to ensure that most of the Lyn that is SH2-bound to receptor aggregates produces phosphorylation, i.e. phosphorylation is faster than dephosphorylation. In the current parameter set the dephosphorylation rate constant is 20 s^{-1} (see **_Interpretation of dephosphorylation kinetics_**, below); therefore the rate constant for β phosphorylation by SH2-bound Lyn ($p^{*}_{L\beta}$) was taken to be 100 s^{-1}. Relative rates of phosphorylation have a much larger effect on model results and are derived from experimental observations. We set rate constants for Lyn-mediated phosphorylation of β, γ, and Syk so that the binding of Lyn's SH2 domain to the phosphorylated β ITAM raises the phosphorylation rate three-fold, consistent with the level of increase in activation measured _in vitro_ when Lyn binds to ITAM phosphopeptides (10, 11). In the model the rate constants for ITAM phosphorylation are for converting an unphosphorylated ITAM to a phosphorylated ITAM that acts as a high affinity docking site. The rate constant for γ ITAM phosphorylation is taken to be thirty times lower than the rate constant for β ITAM phosphorylation because Syk binding requires double phosphorylation of the γ ITAM, and both biochemical and structural evidence indicate a strong preference by Lyn to phosphorylate one of the two γ ITAM tyrosines, the N-terminal tyrosine, suggesting that double phosphorylation is considerably slower than phosphorylation of the first tyrosine (46, 47). The magnitude of the difference in β and γ ITAM phosphorylation rates, i.e., the factor of 30, was determined by requiring that the removal of the high affinity Lyn-receptor interaction has a negative effect on the total amount of Syk autophosphorylation, i.e. that the β ITAM acts as an "amplifier" of signaling (29). The underlying analysis is presented below (see **_The β ITAM can act as an amplifier or inhibitor_**).

Syk is phosphorylated in the model by either Lyn or Syk through transphosphorylation (19, 21, 48). In the model Lyn phosphorylates Syk tyrosines located in the linker region, while Syk phosphorylates the activation loop tyrosines (21). Although Lyn may be responsible _in vivo_ for a small portion of the Syk activation loop

phosphorylation, full Syk activation is achieved only when kinase-active Syk is available (19, 21). In the current model, linker region phosphorylation is used only as a marker and has no effect on Syk activity or binding properties. Recent studies indicate that the four linker region tyrosines have distinct and possibly competing effects that are difficult to lump together (21, 23). The model can be augmented to include such effects as further information becomes available. Activation loop phosphorylation serves as a marker of Syk activation for downstream events and produces a two-fold increase in Syk activity (23).

The last reaction class in Fig. 2 indicates that phosphorylated units that are not protected through association with an SH2 domain can be dephosphorylated, with a common rate constant, d, which we call the "intrinsic" rate constant for dephosphorylation. Dephosphorylation is blocked when an SH2 domain is associated with the phosphorylated site (28). The intrinsic dephosphorylation rate is fit together with the rate constants for Lyn and Syk dissociating from phosphorylated ITAMs to match experimentally-observed dephosphorylation rates (49), as described below in **_Interpretation of dephosphorylation kinetics_**. Good agreement is obtained only when d is much faster than the observed dephosphorylation rate, which is required in order for dephosphorylation to compete with kinase binding. The rate of kinase dissociation from phosphorylated receptors thus effectively controls the observed rate of dephosphorylation in the model.

Model summary

The model we have described consists of a reaction network with 354 distinct chemical species (Fig. 1) and the 3680 chemical reactions (Fig. 2) that connect them. The components and the "wiring" that connects them are based on a large number of biochemical experiments on several different cell types that have been reported in the literature and discussed above. A comparatively small number of rate constants and concentrations (Table 1) parameterize the model and their numerical values are specific to RBL cells. We have written a computer program (50) to generate the states and reaction network from the components and rules given above. This network along with the rate parameters and initial concentrations is passed to a second program that generates

and solves a set of 354 differential equations for the concentration of each chemical species as a function of time using standard methods (51). To compare simulation results with experiments, we add up the concentrations of species with a particular characteristic, e.g. phosphorylated γ ITAM.

Results

We present three types of results: tests of mechanistic assumptions, estimation of unknown parameters, and additional tests to see if model predictions based on the estimated parameters are quantitatively consistent with available data. The results are interrelated. For example, the analysis that addresses the mechanisms underlying the amplification function of the β ITAM is also essential for estimating a key parameter— the rate at which Lyn transphosphorylates both tyrosines in a γ ITAM. Furthermore, all of the parameter values, estimated from multiple experiments, are used in the tests for consistency of model predictions with the data. The following presentation of the interrelated results is organized in terms of different types of experiments.

In the first three subsections we show that, for the parameter estimates summarized in Table 1, the model is quantitatively consistent with RBL cell data on the kinetics of phosphorylation of receptor subunits and Syk, dose-response relations, kinetics of dephosphorylation of receptor subunits, and differences between the γ and β subunits in all three of these types of experiments.

The remaining subsections use the model to predict changes in system behavior in experiments where particular system parameters are altered. We show, by simulating experiments with three ligands that have different dissociation rate constants, that the model predicts behavior indicative of "kinetic proofreading," consistent with observations of Torigoe et al. (42). The other perturbations we consider involve changes in the intracellular content or activity of the interacting molecules. In these cases, our results serve two functions. One is to pin down parameter values that characterize the RBL cell system, since we find that certain changes in parameter values will change the predicted behavior so that it is no longer consistent with RBL cell data. The second function of predicting cell behavior when a parameter is altered is to identify experiments, using appropriate transfectants, to test mechanistic assumptions of the

model (e.g., the assumption that Syk autophosphorylation is intermolecular) or to determine conditions consistent with experimentally-observed behavior (e.g., signal amplification or, potentially, signal inhibition by the β ITAM).

Consistency of the model with phosphorylation kinetics

As a first test of the model, we examine the kinetics of receptor aggregation and tyrosine phosphorylation (Fig. 3) in RBL cells stimulated with covalently-linked dimers of IgE (27). A feature of dimer-induced receptor phosphorylation is that it persists for a long period (at least an hour) rather than rising, going through a maximum, and then decreasing rapidly, as is seen with multivalent antigens (26). At 1.6 nM dimer concentration, receptor aggregation reaches half of its maximum value at about 25 min and is still increasing after 1 hour (Fig. 3a). In contrast, the levels of receptor ITAM phosphorylation plateau at much earlier times in both the experiments and model simulations (Fig. 3b). The times to reach half maximum value in the model under these conditions are 5 min for β phosphorylation and 9 min for γ phosphorylation, values that are comparable to the approximately 10 min time scale observed experimentally.

The kinetics of receptor and Syk phosphorylation in the model are determined by two primary factors. First, ligand-receptor binding is the rate-limiting step, so that except at early times (<1 min) there is a quasi-equilibrium between the number of aggregates and all downstream events. In other words, the amount of receptor or Syk phosphorylation at 10 min is nearly identical to the amount that would be observed at a steady state with the same total number of aggregates. Second, the initiating kinase Lyn is in limited supply, which leads to a saturation of receptor phosphorylation at a relatively low level of aggregation. The current results indicate that when Lyn is limiting, early saturation occurs in β and γ ITAM phosphorylation, as well as Syk phosphorylation. In addition, the model predicts that when the amount of Lyn is increased, phosphorylation increases and saturation of phosphorylation is shifted to later times (simulations not shown). The sensitivity of the model to Lyn concentration and the agreement between experiments and the model predictions at low but not high Lyn concentration provide strong additional support for the contention that Lyn is limiting in RBL cells.

Figure 3b shows that the level of γ phosphorylation exceeds β phosphorylation by about two-fold, in agreement with both previous measurements (27) and current data (see below). A γ ITAM tyrosine that becomes phosphorylated has a longer lifetime than a β phosphotyrosine because the concentration of Syk, which binds to the γ ITAM, is much higher than that of Lyn, which binds to the β ITAM. Protection thus acts as a mechanism to amplify γ phosphorylation in relation to β phosphorylation, and more than compensates for the slower rate at which Lyn phosphorylates γ compared to β. This amplification can be quantified by the ratio of γ to β phosphorylation, which is discussed more in the next section. The increase of this ratio with time and with increasing aggregation causes the shift in the plateau of γ phosphorylation to longer times.

The time course in Fig. 3c shows a rapid redistribution of Lyn, which upon aggregation becomes much more tightly associated with the receptor through binding of its SH2 domain to the phosphorylated β ITAM. At maximum receptor aggregation, about 80% of available Lyn is bound through its SH2 domain to β, which amounts to about 5% of receptors with SH2-bound Lyn. The model predicts about a two-fold increase in the amount of Lyn associated with receptor upon stimulation. Chemical cross-linking experiments have indicated about a three-fold increase in Lyn association upon stimulation (11).

Finally, Fig. 3d shows that the predicted Lyn-mediated and Syk-mediated phosphorylation of Syk have similar kinetics and magnitude. It is unclear at present whether the catalytic activity of unphosphorylated Syk bound to the γ ITAM is sufficient to transphosphorylate an adjacent Syk molecule (23), as assumed by the model, or whether Syk must first be activated by Lyn (19). In any event, the predicted time course of total Syk phosphorylation captures the short time behavior of the experimentally determined time course. At long times Syk phosphorylation drops off while the predicted level plateaus. Since the model does not include components that interact with phosphorylated Syk, such as Cbl (52), discrepancies at long times are not surprising.

Consistency of the model with dose-response curves

Figure 4 shows the results of both simulations and experiments in which we have stimulated RBL cells with varying concentrations of covalently-linked IgE dimers for 10

min. There is good agreement between the simulated and experimental results for receptor and Syk phosphorylation (Fig. 4b,d). The model predicts that phosphorylation in response to aggregation is shifted to lower ligand concentrations than aggregation, and that Syk phosphorylation is shifted farther than receptor phosphorylation. For example, receptor phosphorylation at 2 nM is about 65% of the maximum at higher ligand concentrations, while Syk phosphorylation is about 85% of its maximum value. The experimental results also support this trend. As was the case for the kinetics, simulations with Lyn in excess shift the response to higher aggregate concentrations and fail to achieve reasonable agreement with experiments (simulations not shown).

Figure 4c shows the ratio of γ-phosphorylated receptors to β-phosphorylated receptors, which is determined independently at each concentration. The experimental ratio is consistently higher than the simulated result, although the discrepancy is minimal at high ligand concentrations. In all cases the γ/β ratio is significantly greater than 1, which arises in the model from the fact that there is about ten-fold more Syk than Lyn available to bind and protect phosphotyrosines. The model predicts that the γ/β ratio increases with increasing ligand concentration because the amount of free Lyn available to rebind and protect β phosphotyrosines decreases as the number of aggregates increases, while the amount of free Syk is affected to a much smaller extent.

Interpretation of dephosphorylation kinetics

Mao and Metzger (49) measured the rates of dephosphorylation for the β and γ ITAMs in RBL cells by adding an excess of monovalent hapten to break up aggregates induced by DNP-BSA ligand binding to anti-DNP IgE. We simulated this experiment with our model using the forward rate constants for the IgE dimer while setting the reverse rate constants k_{-1} and k_{-2} to 0.5 s^{-1}. Setting the ligand concentration to 1.7 nM for two minutes induces about 5% of the receptors to form dimers. Hapten addition is then modeled by setting the ligand forward rate constants to zero, allowing the dimers to break up but not re-form. We fit three model parameters, the intrinsic dephosphorylation rate constant, d, the rate constant for Lyn dissociating from the phosphorylated β ITAM, k^*_{-L}, and a common rate constant for activated or non-activated Syk dissociating from the phosphorylated γ ITAM, $k_{-S} = k^*_{-S}$, to match the observed dephosphorylation rates (49) of

17

0.12 s^{-1} for β and 0.06 s^{-1} for γ. Results of the fit are shown in Fig. 5. Good agreement is obtained only when d is much higher than the observed rate of dephosphorylation, d_{obs}. This result can be explained by a simple three-state model of dephosphorylation,

$$\text{R-P-E} \underset{k_{+E}E}{\overset{k_{-E}}{\rightleftharpoons}} \text{R-P} \xrightarrow{d} \text{R} ,$$
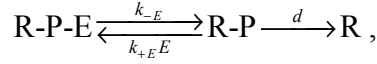
where R is receptor, R-P is phosphorylated receptor and R-P-E is enzyme-bound phosphorylated receptor. At steady state

$$d_{obs} = \frac{k_{-E}}{1 + k_{+E}E/d} \tag{1}$$

and thus the observed dephosphorylation rate is limited by the kinase dissociation rate, k_{-E}. In addition, d_{obs} will be slower than k_{-E} if d cannot compete with the rate of kinase binding, $k_{+E}E$. In the current model the maximum rate of kinase binding, $k_{+E}E$, is 1.4 s^{-1} for Lyn and 24 s^{-1} for Syk. The thin dashed lines in Fig. 5 show that setting d to a value of 0.12 s^{-1} (the experimentally observed rate of β dephosphorylation) results in very slow dephosphorylation rates in the model, as expected from Eq. (1). In our fits the equilibrium constant, $K_E = k_{+E}/k_{-E}$, was fixed, which places the lower limit on d of $d_{obs}K_E E$ or about 11 s^{-1} for Syk. The fit shown in Fig. 5 was obtained by setting d=20 s^{-1} and adjusting the kinase dissociation rates to match d_{obs} from experiment (49). For these parameters R-P has about an equal chance of binding Syk or being dephosphorylated, and dephosphorylation occurs at about half the rate of Syk dissociation. Changing the enzyme concentration affects this balance and changes both the observed rate of dephosphorylation and the level of phosphorylation achieved at steady state, as we investigate below. Figure 5 shows that reducing either of the kinase concentrations 10-fold increases the apparent rate of dephosphorylation, but not to the level of either the aggregate breakup rate (1 s^{-1}) or the intrinsic dephosphorylation rate (20 s^{-1}). Thus the effects of protection can be expected to persist even at relatively low kinase concentrations.

Concentration of Syk available for receptor binding

Changing the Syk concentration in the model can affect early signaling events in two primary ways: increasing the concentration of Syk SH2 domains can lead to

increased γ ITAM phosphorylation through protection of ITAM tyrosines from dephosphorylation (as described above), and increasing the concentration of the Syk kinase domain can lead to increased Syk activation through autophosphorylation. The first effect is demonstrated in Fig. 6a, which shows the increase in the ratio of γ to β phosphorylation as the Syk concentration in the model is increased. The γ/β phosphorylation ratio measured experimentally at the corresponding ligand concentration lies in the range of 2–3, which occurs in the model at a Syk concentration where the total number of Syk molecules available to interact with phosphorylated receptors is close to the total number of receptors. For the model to be consistent with the data, the number of Syk molecules available to receptors must be close to the assayed number of Syk molecules per cell, in contrast to the situation with Lyn, where the availability of Lyn within the receptor compartment appears to be much lower than its overall concentration within the cell (3). Because bound Syk protects γ ITAM phosphotyrosines from phosphatases, the abundance of available Syk has the effect of increasing double phosphorylation of the γ ITAM to a much higher level than can be maintained through the action of Lyn alone.

The results of the model for receptor phosphorylation can also be compared with the experimental results of Scharenberg et al. (53), who observed an increase in receptor phosphorylation of antigen-stimulated RBL cells transfected with porcine Syk or truncated porcine Syk protein that contained only the Syk tandem SH2 domains, as compared with antigen-stimulated untransfected RBL cells. The fact that increased phosphorylation was observed when only the truncated Syk was expressed was taken as evidence that the increase in phosphorylation could not be attributed to direct receptor phosphorylation by Syk but rather to protection of phosphotyrosines from dephosphorylation by the binding of Syk SH2 domains. The model results shown in Fig. 6a strongly support this interpretation (since Syk does not phosphorylate the receptor in the model) and demonstrate that the predicted dose-response relationship between Syk concentration and receptor ITAM phosphorylation arising from this mechanism is maintained over a range of Syk concentrations spanning at least three orders of magnitude. Note that the predicted change in the γ/β ratio shown in Fig. 6a is entirely the result of increasing the γ ITAM phosphorylation; the level of β phosphorylation is

19

unaffected by the Syk concentration because, in the model, Syk binds only to the phosphorylated γ ITAM. Scharenberg et al. also observed an increase in phosphorylation of the β ITAMs upon overexpression of Syk, which suggests that at very high Syk concentrations, Syk SH2 domains may bind and protect the β ITAM phosphotyrosines as well.

Figure 6b shows that the efficiency of Syk activation, measured as the fraction of Syk molecules that are activated upon stimulation, peaks at about 0.12, when the number of Syk molecules is about 10% of the number of receptors. The value when the number of Syk molecules is equal to the number of receptors is about 0.05, consistent with our experimental measurement of 0.06 for RBL cell stimulation with covalently cross-linked IgE dimers.

Effect of Lyn concentration on the γ/β phosphorylation ratio

In contrast to variation of the γ/β phosphorylation ratio with Syk concentration (Fig. 6a), increasing the Lyn concentration decreases the predicted γ/β phosphorylation ratio over a broad concentration range (Fig. 6c). The experimentally observed ratio is consistent with the concentration of Lyn available to receptors being about 5–10% of the number of receptors, as estimated previously based on the kinetics of total receptor phosphorylation (3). The change in the γ/β phosphorylation ratio with Syk concentration resulted solely from Syk's role in protecting γ phoshotyrosines from dephosphorylation. Dependence of the γ/β phosphorylation ratio on the Lyn concentration is complicated by the fact that Lyn affects both β and γ phosphorylation and the fact that Lyn has two types of interaction with the β subunit.

Mechanism of Syk autophosphorylation

In the model we have presented, the mechanism for Syk autophosphorylation is transphosphorylation. A Syk molecule bound to one receptor in an aggregate phosphorylates a Syk bound to the other receptor (Fig. 2). This hypothesis seems reasonable because transphosphorylation has been established as the primary mechanism of tyrosine phosphorylation of the epidermal growth factor receptor and other receptor kinases (54) and FcεRI (15). On the other hand, although Lyn acts on receptor ITAMs by

transphosphorylation, the juxtaposition of two Lyn molecules in a receptor aggregate is not required for Lyn to be active (27). The analysis in (27) depended on the experimental observation of a linear relation between the amounts of Lyn in a series of stable transfectants and the extent of ITAM phosphorylation, i.e., phosphorylation was simply proportional to the amount of Lyn. The relation would have been quadratic, i.e., phosphorylation would have been proportional to the square of the concentration of available Lyn, if juxtaposition of two Lyns were required. With appropriate transfectants, similar methods could be used to test the hypothesis that phosphorylation of Syk tyrosines by Syk is transphosphorylation. Figure 7 shows what the current model predicts for experiments with transfectants having different amounts of Lyn and Syk. Syk autophosphorylation would depend quadratically on the concentrations of both Lyn (Fig. 7a) and Syk (Fig. 7b).

How would alternative findings be interpreted? If Syk autophosphorylation varies linearly with the cellular content of Syk, we would have to consider a model where the kinase domain of a Syk molecule phosphorylates tyrosines in the activation loop of the same molecule. If Syk autophosphorylation varies quadratically with the concentration of Syk but linearly with the concentration of Lyn, we would consider a model where, when Lyn phosphorylates a γ dimer, two Syks can bind to the dimer. As discussed earlier, we assumed for steric reasons that only one Syk can bind to the γ dimer, but this assumption can be modified if there is evidence to the contrary. A linear dependence of the level of phosphorylation of specific Syk tyrosines on the concentration of Lyn could also indicate that the residues examined are phosphorylated primarily by Lyn, not by Syk.

Variation of aggregate lifetime: Evidence for kinetic proofreading

A number of recent experimental and theoretical models have shown that one major criterion by which signaling pathways discriminate between different ligands is the lifetime of the ligand–receptor bond (42, 55-63). The basic idea behind this "kinetic proofreading," in analogy to similar mechanisms in biosynthetic pathways (64), is that rapidly dissociating ligands are less effective than slowly dissociating ligands in stimulating downstream signaling events that require completion of a sequence of biochemical reactions while the supramolecular complex of ligand, receptors, and

associated signaling molecules remains intact. A key assumption is that the entire complex dissociates and biochemical modifications are reversed rapidly once the ligand dissociates. Thus, the ligand-receptor bond serves as a timer for downstream signaling events, and ligands with short lifetimes will be ineffective at triggering events that require longer times to commence.

We test whether our model exhibits the basic features of kinetic proofreading by comparing the levels of receptor and Syk phosphorylation achieved by three different hypothetical bivalent ligands with the same forward rate constants (k_{+1} and k_{+2}) but different dissociation rate constants (k_{-1} and k_{-2}). To equalize the comparison, the levels of phosphorylation are plotted as a function of the number of aggregates formed. The top panel of Fig. 8 shows that for each ten-fold increase in the ligand dissociation rate constants, the ligand concentration must be raised approximately 100-fold to maintain the same level of aggregation. As the ligand affinity decreases, the maximum number of aggregates that may be formed also decreases, restricting the range of comparison. The results shown in the bottom three panels of Fig. 8 show that proximal events, represented by β and γ phosphorylation, are affected much less by the change in ligand-receptor lifetime than Syk autophosphorylation, which is the furthest downstream event in our model. The effect of kinetic proofreading on Syk activation is particularly dramatic at low ligand concentrations—there is more than a 100-fold change in the level of activation going from the medium affinity ligand to the low affinity ligand.

Interestingly, the extent of kinetic proofreading is predicted to decrease as the ligand concentration goes up, and there is even a crossover for γ phosphorylation at high concentrations. This effect can be explained as follows. The level of phosphorylation can be enhanced by increasing the mobility of kinases. For example, increasing the dissociation rate constant for constitutively associated Lyn in the model (k_{-L}) actually increases the levels of β and γ phosphorylation at high aggregate concentrations because each Lyn can phosphorylate more than one receptor. An analogous phenomenon, known as "serial engagement" (65, 66), is observed in T cell signaling in which a single MHC-peptide can stimulate a substantial number of T cell receptors. Increasing the ligand-receptor dissociation rate effectively increases the mobility of kinases associated with the receptor. The time for an uncomplexed receptor to join an aggregate decreases as the

ligand concentration is increased, and thus the enhancement of phosphorylation from increased kinase mobility competes more effectively with kinetic proofreading at the highest ligand concentrations. This mechanism demonstrates an exception to the standard assumption in kinetic proofreading models that dissociation of the ligand leads to the complete reversal of all receptor modifications made during the lifetime of the aggregate.

The β ITAM can act as an amplifier or inhibitor

The β subunit has been called an "amplifier" of FcεRI signaling both because $\alpha\beta\gamma_2$ receptors produce a much stronger signal in response to stimulation than $\alpha\gamma_2$ receptors (29) and because expression of the β subunit greatly increases receptor expression at the cell surface (67). One reason that the β subunit might act as a signal amplifier is the specific high-affinity interaction between Lyn's SH2 domain and the phosphorylated β ITAM (40).

Two studies have directly addressed the effect of this interaction. Lin et al. observed an approximately 7-fold reduction in γ ITAM phosphorylation when the three β ITAM tyrosines were mutated to phenylalanine in receptors transfected into NIH-3T3 cells (29) . By comparison, the reduction in γ ITAM phosphorylation was about 20-fold when the entire β subunit was removed from the receptor (29). One difficulty in assessing the importance of the high affinity interaction in this study is the possibility that the low-affinity interaction of Lyn with the receptor is also affected by changes in the β ITAM. Another approach was taken by Honda et al., who transfected various Lyn constructs lacking the C-terminal region into RBL cells and used overexpression of Cbp (C-terminal Src kinase binding protein) to suppress the activity of endogenous Lyn (68). They found that deletion of Lyn's SH2 domain produced only a modest decrease in receptor phosphorylation but nearly eliminated Syk phosphorylation and other downstream events. The authors attributed these results to a form of kinetic proofreading arising from the disruption of the high affinity Lyn–receptor interaction. According to this hypothesis, the low affinity interaction was sufficient to produce a significant level of

receptor phosphorylation, but later events were disrupted by the short lifetime of the Lyn-receptor interaction.

Figure 9 shows the effect of removing the high affinity Lyn-receptor interaction from the model on γ ITAM and Syk phosphorylation. This is accomplished by simply setting the rate constant for β phosphorylation by Lyn ($p_{L\beta}$) to zero. The results are reported in terms of the gain produced by including the high affinity interaction. The gain is defined as the ratio of the phosphorylation when the ITAM is present to the phosphorylation if the ITAM is effectively absent. As observed by Honda et al. (68), the gain for the downstream Syk autophosphorylation is greater than for γ phosphorylation at all ligand concentrations (Fig. 9a). The magnitude of both gains, however, exhibits a strong concentration dependence, and at the highest ligand concentrations the high-affinity interaction acts as a slight inhibitor of γ phosphorylation. These results cannot be explained by kinetic proofreading alone. The amount of downstream phosphorylation induced by Lyn may be written as the product of two terms: the average number of Lyn molecules per aggregrate and the average efficiency of each Lyn in an aggregate at producing the event, e.g. the amount of Syk autophosphorylation divided by the amount of Lyn in aggregates. The gain for Lyn recruitment plotted in Fig. 9a shows that most of the gain for Syk autophosphorylation and its strong concentration dependence can be attributed to the enhanced recruitment of Lyn into aggregates through the high affinity Lyn-receptor interaction. The fact that the gain for Syk autophosphorylation and Lyn association match closely demonstrates that the relative efficiency for the production of autophosphorylated Syk is nearly the same for the high and low affinity interactions of Lyn with β. As was the case with ligand-receptor lifetimes, there is a competition between the effect of kinetic proofreading, which favors the high-affinity interaction, and serial engagement, which favors the low-affinity interaction. For the proximal event, γ phosphorylation, serial engagement dominates, while for Syk autophosphorylation there is a nearly equal balance of the two effects. It thus appears that for the current model parameters the predominant effect of the high affinity interaction is not kinetic proofreading but selective recruitment of Lyn to aggregates.

This balance between kinetic proofreading and serial engagement in the Lyn-receptor interaction can be shifted by varying the rate constants for γ phosphorylation by

24

Lyn, $p_{L\gamma}$ and $p^*_{L\gamma}$, as shown in Fig. 9b. Changing these parameters changes the length of time Lyn must stay associated with the receptor in order to propagate the signal downstream but does not affect the Lyn-receptor interaction. Decreasing the phosphorylation rate constants increases the effect of kinetic proofreading, leading to larger gains for both γ phosphorylation and Syk autophosphorylation. For moderate increases in the rate constants, on the other hand, serial engagement becomes dominant and the high affinity interaction becomes an inhibitor of both γ and Syk phosphorylation.

Discussion

We developed a detailed kinetic model for the early events in FcεRI-mediated signaling, from receptor-ligand binding through the autophosphorylation of Syk. We applied the model to extract quantitative and qualitative information from new and published data and to identify additional experiments that can be used to test the model and to improve estimates of key parameters.

The model is "detailed" in the sense that it describes events at the molecular level, including ligand-induced aggregation of receptors (FcεRI), association of receptor subunits (β and γ) with two protein tyrosine kinases (Lyn and Syk), and phosphorylation and dephosphorylation of specified sets of tyrosines on β, γ, and Syk. The model makes predictions as a function of time, ligand concentration, concentrations of signaling components, and potential experimental modifications of the interacting proteins (e.g. removal or impairment of a domain). The last area is particularly important because so much of what we know about signaling pathways comes from genetic manipulation of the components. The model provides a tool for interpreting such experiments and designing new ways to use genetically altered proteins to test ideas about molecular interactions and signaling mechanisms.

The model, with the parameters in Table 1, is consistent with a variety of experimental data. Simulations of experiments where RBL cells were exposed to covalently cross-linked dimers of IgE reproduced the observed kinetics of phosphorylation of receptor subunits over a period of an hour (Fig. 3). Theoretical and experimental dose-response curves also matched closely (Fig. 4). Model-based

25

simulations also agreed with the observed kinetics of dephosphorylation of the β and γ ITAMs (Fig. 5).

Some of the parameters in Table 1 were determined directly in previously reported and new experiments. We estimated other parameters based on the fit of model predictions to data. The data impose severe constraints on the parameters. The constraints carry biological information, for example information about the control of ITAM dephosphorylation and the availability of kinases.

The Lyn and Syk concentrations that are parameters in the model represent the numbers of molecules of Lyn and Syk available to interact with FcεRI. The amount of available Lyn and Syk may be less than the total number per cell. Previously, we analyzed time courses of phosphorylation of FcεRI in RBL cells using a model that included only Lyn and the receptor (3). The analysis led us to propose that the amount of Lyn available to interact with the receptor was considerably less than the total cellular Lyn. Subsequent experiments involving competition for Lyn among different populations of receptor aggregates were consistent with Lyn being limiting (41). Here, using the expanded model, we presented additional evidence that Lyn is limiting. In contrast, we showed here that the amount of Syk available to interact with the receptor is comparable to total cellular Syk. We measured the total number of Syk molecules in RBL cells and found that it is close to the measured number of FcεRI. We showed that all or most of that Syk must be available to the receptors for the model to be consistent with differences between β and γ ITAM phosphorylation levels (Figs. 3 and 4) and differences in the rates of β and γ ITAM dephosphorylation (Fig. 5).

With regard to the control of ITAM dephosphorylation, the key parameters are the intrinsic rate constant for dephosphorylation and parameters that characterize protection from dephosphorylation when Lyn binds to a phosphorylated β ITAM or Syk binds to a doubly phosphorylated γ ITAM. Therefore the concentrations of available Lyn and Syk, as well as rate constants for Lyn and Syk association and dissociation, can influence the experimentally observed time course of ITAM dephosphorylation. We showed that in the RBL cell system these parameters have a strong effect. The intrinsic rate of dephosphorylation must be two to three hundred times faster than the apparent rate to reproduce the dephosphorylation results of Mao and Metzger (49). If the intrinsic rate

were lower, dephosphorylation would not compete effectively with kinase binding and little dephosphorylation would be observed (Fig. 5).

Qualitative aspects of signaling can depend sensitively and in non-obvious ways on parameters. Experiments have shown that the β subunit acts to amplify signaling through FcεRI (29). Experiments in RBL cells demonstrate the role of β ITAM phosphorylation in signal amplification (68). We showed, by comparing model predictions in the presence and absence of β ITAM phosphorylation that amplification depends on the rate at which Lyn transphosphorylates the γ ITAM. If transphosphorylation of γ is fast enough for constitutively bound Lyn to phosphorylate γ efficiently, but the high affinity interaction of Lyn with the phosphorylated β ITAM keeps Lyn from dissociating rapidly and moving on to phosphorylate other receptors, then the model predicts that the high affinity interaction will be inhibitory (see Fig. 9, second panel). In Table 1, the rate at which Lyn transphosphorylates the γ ITAM is set so that the β ITAM is an amplifier of signaling.

We have summarized the utility of the model for quantitative prediction, which depends on accurate estimation of parameters and feeds back, through comparison of model predictions with data, to improve parameter estimates. Another use of a detailed model is to test simplified models, to determine conditions under which a simplified model makes valid predictions as well as conditions when the results may be misleading. We have shown that the cellular responses in the model depend on the lifetime of the ligand-receptor bond in a way that is qualitatively consistent with the predictions of simplified "kinetic proofreading" models (Fig. 8). Quantitative predictions of the detailed model provide a standard of comparison for predictions from kinetic proofreading models and, potentially, clarify the biological interpretation of estimated kinetic proofreading parameters.

One function of a mathematical model is to identify new experiments to test biological ideas. A question that remains open is whether autophosphorylation of Syk is intra- or intermolecular. The model postulates that both Lyn and Syk, associated with one FcεRI in an aggregate, can only transphosphorylate Syk associated with a second receptor in the aggregate. Therefore in the model, autophosphorylation of Syk is intermolecular. Based on the analysis of the model, we suggest a quantitative method for

distinguishing among models where autophosphorylation requires only one Syk acting intramolecularly, two Syks associated with a γ dimer on a single receptor, or two Syks associated with distinct receptors in an aggregate.

So far, the model provides a consistent picture of RBL cell signaling induced by IgE dimers without incorporating spatial effects, in particular the role of specialized lipid domains and the redistribution of receptors and kinase molecules during signaling (69-73). In the experimental system we have analyzed, phosphorylation of FcεRI and Syk is maintained dynamically, with rapid dephosphorylation balanced by continued phosphorylation for at least an hour (26, 27). It is possible that dimers do not induce the redistribution of Lyn away from receptors and Syk that has been observed when signaling is initiated by multivalent antigen (74).

In the model, only Lyn phosphorylates receptor ITAMs. Recently it has been demonstrated that a second Src kinase, Fyn, associates with FcεRIβ and plays a key role in mast cell degranulation (75). Fyn is recruited to aggregated FcεRI (75), but whether Fyn competes with Lyn for sites on the receptor is unknown. What role, if any, Fyn plays in ITAM phosphorylation also remains to be elucidated.

A detailed model of a cell signaling cascade will always be a work in progress. Analysis of such a model identifies additional experimental measurements and qualitative manipulations needed to distinguish mechanisms and provide accurate quantitative predictions. The experimental results identify points where the model or the parameter estimates must be modified. Ultimately we want sufficient knowledge for quantitative prediction of larger segments of signaling pathways. To have confidence in such predictions, our approach is to proceed step-wise, testing each extension of the model against many different forms of experimental data.

Acknowledgments

References

1.   Hunter, T. 2000. Signaling–2000 and beyond. *Cell 100:113*.
2.   Ray, L., L. Chong, and N. Gough. 2002. Computational biology. *Science's STKE http://stke.sciencemag.org/cgi/content/full/sigtrans;2002/148/eg10*.
3.   Wofsy, C., C. Torigoe, U. M. Kent, H. Metzger, and B. Goldstein. 1997. Exploiting the difference between intrinsic and extrinsic kinases: Implications for regulation of signaling by immunoreceptors. *J. Immunol. 159:5984*.
4.   Wofsy, C., B. M. Vonakis, H. Metzger, and B. Goldstein. 1999. One Lyn molecule is sufficient to initiate phosphorylation of aggregated high-affinity IgE receptors. *Proc. Natl. Acad. Sci. U. S. A. 96:8615*.
5.   Goldstein, B., J. R. Faeder, W. S. Hlavacek, M. L. Blinov, A. Redondo, and C. Wofsy. 2002. Modeling the early signaling events mediated by FcεRI. *Mol. Immunol. 38:1213*.
6.   Keegan, A. D., and W. E. Paul. 1992. Multichain immune recognition receptors: Similarities in structure and signaling pathways. *Immunol. Today 13:63*.
7.   Reth, M. 1989. Antigen receptor tail clue. *Nature 338:383*.
8.   Cambier, J. C. 1995. Antigen and Fc receptor signaling: The awesome power of the immunoreceptor tyrosine-based activation motif (ITAM). *J. Immunol. 155:3281*.
9.   Kinet, J. P. 1999. The high-affinity IgE receptor (FcεRI): From physiology to pathology. *Annu. Rev. Immunol. 17:931*.
10.   Eiseman, E., and J. B. Bolen. 1992. Engagement of the high-affinity IgE receptor activates Src protein-related tyrosine kinases. *Nature 355:78*.
11.   Yamashita, T., S. Y. Mao, and H. Metzger. 1994. Aggregation of the high-affinity IgE receptor and enhanced activity of p53/p56^{lyn} protein-tyrosine kinase. *Proc. Natl. Acad. Sci. U. S. A. 91:11251*.
12.   Jouvin, M. H. E., M. Adamczewski, R. Numerof, O. Letourneur, A. Valle, and J. P. Kinet. 1994. Differential control of the tyrosine kinases Lyn and Syk by the 2 signaling chains of the high-affinity immunoglobulin-E receptor. *J. Biol. Chem. 269:5918*.
13.   Vonakis, B. M., H. X. Chen, H. HaleemSmith, and H. Metzger. 1997. The unique domain as the site on Lyn kinase for its constitutive association with the high affinity receptor for IgE. *J. Biol. Chem. 272:24072*.
14.   Vonakis, B. M., H. Haleem-Smith, P. Benjamin, and H. Metzger. 2001. Interaction between the unphosphorylated receptor with high affinity for IgE and Lyn kinase. *J. Biol. Chem. 276:1041*.
15.   Pribluda, V. S., C. Pribluda, and H. Metzger. 1994. Transphosphorylation as the mechanism by which the high-affinity receptor for IgE is phosphorylated upon aggregation. *Proc. Natl. Acad. Sci. U. S. A. 91:11246*.
16.   Nishizumi, H., and T. Yamamoto. 1997. Impaired tyrosine phosphorylation and Ca_2^+ mobilization, but not degranulation, in Lyn-deficient bone marrow-derived mast cells. *J. Immunol. 158:2350*.
17.   Hutchcroft, J. E., R. L. Geahlen, G. G. Deanin, and J. M. Oliver. 1992. FcεRI-mediated tyrosine phosphorylation and activation of the 72-kDa protein-tyrosine kinase, PTK72, in RBL-2H3 rat-tumor mast cells. *Proc. Natl. Acad. Sci. U. S. A. 89:9107*.

18.   Benhamou, M., N. J. P. Ryba, H. Kihara, H. Nishikata, and R. P. Siraganian. 1993. Protein-tyrosine kinase p72^{syk} in high-affinity IgE receptor signaling: Identification as a component of pp72 and association with the receptor γ-chain after receptor aggregation. *J. Biol. Chem. 268:23318*.

19.   El-Hillal, O., T. Kurosaki, H. Yamamura, J. P. Kinet, and A. M. Scharenberg. 1997. Syk kinase activation by a src kinase-initiated activation loop phosphorylation chain reaction. *Proc. Natl. Acad. Sci. U. S. A. 94:1919*.

20.   Keshvara, L. M., C. Isaacson, M. L. Harrison, and R. L. Geahlen. 1997. Syk activation and dissociation from the B-cell antigen receptor is mediated by phosphorylation of tyrosine 130. *J. Biol. Chem. 272:10377*.

21.   Keshvara, L. M., C. C. Isaacson, T. M. Yankee, R. Sarac, M. L. Harrison, and R. L. Geahlen. 1998. Syk- and Lyn-dependent phosphorylation of Syk on multiple tyrosines following B cell activation includes a site that negatively regulates signaling. *J. Immunol. 161:5276*.

22.   Siraganian, R. P., J. Zhang, K. Suzuki, and K. Sada. 2002. Protein tyrosine kinase Syk in mast cell signaling. *Mol. Immunol. 38:1229*.

23.   Zhang, J., M. L. Billingsley, R. L. Kincaid, and R. P. Siraganian. 2000. Phosphorylation of Syk activation loop tyrosines is essential for Syk function: An in vivo study using a specific anti-Syk activation loop phosphotyrosine antibody. *J. Biol. Chem. 275:35442*.

24.   Zhang, J., T. Kimura, and R. P. Siraganian. 1998. Mutations in the activation loop tyrosines of protein tyrosine kinase Syk abrogate intracellular signaling but not kinase activity. *J. Immunol. 161:4366*.

25.   Segal, D. M., J. D. Taurog, and H. Metzger. 1977. Dimeric immunoglobulin-E serves as a unit signal for mast-cell degranulation. *Proc. Natl. Acad. Sci. U. S. A. 74:2993*.

26.   Kent, U. M., S. Y. Mao, C. Wofsy, B. Goldstein, S. Ross, and H. Metzger. 1994. Dynamics of signal-transduction after aggregation of cell-surface receptors: Studies on the type-I receptor for IgE. *Proc. Natl. Acad. Sci. U. S. A. 91:3087*.

27.   Wofsy, C., U. M. Kent, S. Y. Mao, H. Metzger, and B. Goldstein. 1995. Kinetics of tyrosine phosphorylation when IgE dimers bind to Fcε receptors on rat basophilic leukemia-cells. *J. Biol. Chem. 270:20264*.

28.   Rotin, D., B. Margolis, M. Mohammadi, R. J. Daly, G. Daum, N. Li, E. H. Fischer, W. H. Burgess, A. Ullrich, and J. Schlessinger. 1992. SH2 domains prevent tyrosine dephosphorylation of the EGF receptor: Identification of tyr992 as the high-affinity binding-site for SH2 domains of phospholipase C-γ. *Embo Journal 11:559*.

29.   Lin, S. Q., C. Cicala, A. M. Scharenberg, and J. P. Kinet. 1996. The FcεRIβ subunit functions as an amplifier of FcεRIγ-mediated cell activation signals. *Cell 85:985*.

30.   Péneff, C., M.-P. Lefranc, and P. Dariavach. 2000. Characterisation and specificity of two single-chain Fv antibodies directed to the protein tyrosine kinase Syk. *J. Immunol. Methods 236:105*.

31.   Hlavacek, W. S., A. S. Perelson, B. Sulzer, J. Bold, J. Paar, W. Gorman, and R. G. Posner. 1999. Quantifying aggregation of IgE-FcεRI by multivalent antigen. *Biophys. J. 76:2421*.

32. Posner, R. G., B. Lee, D. H. Conrad, D. Holowka, B. Baird, and B. Goldstein. 1992. Aggregation of IgE receptor complexes on rat basophilic leukemia-cells does not change the intrinsic affinity but can alter the kinetics of the ligand IgE interaction. *Biochemistry 31:5350.*

33. Rivera, J., J.-P. Kinet, J. Kim, C. Pucillo, and H. Metzger. 1988. Studies with a monoclonal antibody to the β subunit of the receptor with high affinity for immunoglobulin E. *Mol. Immunol. 25:247.*

34. Chen, T., B. Repetto, R. Chizzonite, C. Pullar, C. Burghardt, E. Dharm, Z. Zhao, R. Carroll, P. Nunes, M. Basu, W. Danho, M. Visnick, J. Kochan, D. Waugh, and A. M. Gilfillan. 1996. Interaction of phosphorylated FcεRIγ immunoglobulin receptor tyrosine activation motif-based peptides with dual and single SH2 domains of p72^{syk}: Assessment of binding parameters and real, time binding kinetics. *J. Biol. Chem. 271:25308.*

35. http://www.basic.nwu.edu/biotools/proteincalc.html

36. Amoui, M., L. Dráberová, P. Tolar, and P. Dráber. 1997. Direct interaction of Syk and Lyn protein tyrosine kinases in rat basophilic leukemia cells activated via type I Fcε receptors. *Eur. J. Immunol. 27:321.*

37. Metzger, H., S. Eglite, H. Haleem-Smith, I. Reischl, and C. Torigoe. 2002. Quantitative aspects of signal transduction by the receptor with high affinity for IgE. *Mol. Immunol. 38:1207.*

38. Nadler, J. S., S. A. Matthews, M. Turner, and J. P. Kinet. 2001. Signal transduction by the high-affinity immunoglobulin E receptor FcεRI: Coupling form to function. *Adv. Immunol. 76:325.*

39. Subramanian, K. 1995. Binding and functional effects of defined ligands with monovalent, bivalent, and bispecfic IgE in solution and on the cell surface. PhD thesis, Cornell University, Ithaca, NY.

40. Kihara, H., and R. P. Siraganian. 1994. Src homology-2 domains of Syk and Lyn bind to tyrosine-phosphorylated subunits of the high-affinity IgE receptor. *J. Biol. Chem. 269:22427.*

41. Torigoe, C., B. Goldstein, C. Wofsy, and H. Metzger. 1997. Shuttling of initiating kinase between discrete aggregates of the high affinity receptor for IgE regulates the cellular response. *Proc. Natl. Acad. Sci. U. S. A. 94:1372.*

42. Torigoe, C., J. K. Inman, and H. Metzger. 1998. An unusual mechanism for ligand antagonism. *Science 281:568.*

43. Shiue, L., J. Green, O. M. Green, J. L. Karas, J. P. Morgenstern, M. K. Ram, M. K. Taylor, M. J. Zoller, L. D. Zydowsky, J. B. Bolen, and J. S. Brugge. 1995. Interaction of p72^{syk} with the γ-subunits and β-subunits of the high-affinity receptor for immunoglobulin-E, FcεRI. *Mol. Cell. Biol. 15:272.*

44. Ottinger, E. A., M. C. Botfield, and S. E. Shoelson. 1998. Tandem SH2 domains confer high specificity in tyrosine kinase signaling. *J. Biol. Chem. 273:729.*

45. Grucza, R. A., K. Futterer, A. C. Chan, and G. Waksman. 1999. Thermodynamic study of the binding of the tandem-SH2 domain of the Syk kinase to a dually phosphorylated ITAM peptide: Evidence for two conformers. *Biochemistry 38:5024.*

46.   Pao, L. I., S. A. Famiglietti, and J. C. Cambier. 1998. Asymmetrical phosphorylation and function of immunoreceptor tyrosine-based activation motif tyrosines in B cell antigen receptor signal transduction. *J. Immunol. 160:3305*.

47.   Gaul, B. S., M. L. Harrison, R. L. Geahlen, R. K. Burton, and C. B. Post. 2000. Substrate recognition by the Lyn protein-tyrosine kinase: NMR structure of the immunoreceptor tyrosine-based activation motif signaling region of the B cell antigen receptor. *J. Biol. Chem. 275:16174*.

48.   Rivera, V. M., and J. S. Brugge. 1995. Clustering of Syk is sufficient to induce tyrosine phosphorylation and release of allergic mediators from rat basophilic leukemia-cells. *Mol. Cell. Biol. 15:1582*.

49.   Mao, S. Y., and H. Metzger. 1997. Characterization of protein-tyrosine phosphatases that dephosphorylate the high affinity IgE receptor. *J. Biol. Chem. 272:14067*.

50.   Both programs are available at http://cellsignaling.lanl.gov.

51.   Hindmarsh, A. C. 1983. ODEPACK: A systematized collection of ODE solvers. In *Scientific computing*. R. S. Stepleman, ed. North-Holland, Amsterdam, p. 55.

52.   Ota, Y., and L. E. Samelson. 1997. The product of the proto-oncogene c-cbl: A negative regulator of the Syk tyrosine kinase. *Science 276:418*.

53.   Scharenberg, A. M., S. Q. Lin, B. Cuenod, H. Yamamura, and J. P. Kinet. 1995. Reconstitution of interactions between tyrosine kinases and the high-affinity IgE receptor which are controlled by receptor clustering. *Embo Journal 14:3385*.

54.   Lemmon, M. A., and J. Schlessinger. 1994. Regulation of signal-transduction and signal diversity by receptor oligomerization. *Trends Biochem. Sci. 19:459*.

55.   McKeithan, T. W. 1995. Kinetic proofreading in T-cell receptor signal-transduction. *Proc. Natl. Acad. Sci. U. S. A. 92:5042*.

56.   Liu, Z. J., H. Haleem-Smith, H. X. Chen, and H. Metzger. 2001. Unexpected signals in a system subject to kinetic proofreading. *Proc. Natl. Acad. Sci. U. S. A. 98:7289*.

57.   Hlavacek, W. S., A. Redondo, C. Wofsy, and B. Goldstein. 2002. Kinetic proofreading in receptor-mediated transduction of cellular signals: Receptor aggregation, partially activated receptors, and cytosolic messengers. *Bull. Math. Biol. 64:887*.

58.   Hlavacek, W. S., A. Redondo, H. Metzger, C. Wofsy, and B. Goldstein. 2001. Kinetic proofreading models for cell signaling predict ways to escape kinetic proofreading. *Proc. Natl. Acad. Sci. U. S. A. 98:7295*.

59.   Germain, R. N. 2001. The T cell receptor for antigen: Signaling and ligand discrimination. *J. Biol. Chem. 276:35223*.

60.   Coombs, D., A. M. Kalergis, S. G. Nathenson, C. Wofsy, and B. Goldstein. 2002. Activated TCRs remain marked for internalization after dissociation from pMHC. *Nat. Immunol. 3:926*.

61.   Rivera, J., R. Arudchandran, C. Gonzalez-Espinosa, T. S. Manetz, and S. Xirasagar. 2001. A perspective: Regulation of IgE receptor-mediated mast cell responses by a LAT-organized plasma membrane-localized signaling complex. *Int. Arch. Allergy Immunol. 124:137*.

62.   Rosette, C., G. Werlen, M. A. Daniels, P. O. Holman, S. M. Alam, P. J. Travers, N. R. J. Gascoigne, E. Palmer, and S. C. Jameson. 2001. The impact of duration

versus extent of TCR occupancy on T cell activation: A revision of the kinetic proofreading model. *Immunity 15:59*.

63. Swain, P. S., and E. D. Siggia. 2002. The role of proofreading in signal transduction specificity. *Biophys. J. 82:2928*.

64. Hopfield, J. J. 1974. Kinetic proofreading: New mechanism for reducing errors in biosynthetic processes requiring high specificity. *Proc. Natl. Acad. Sci. U. S. A. 71:4135*.

65. Valitutti, S., S. Muller, M. Cella, E. Padovan, and A. Lanzavecchia. 1995. Serial triggering of many T-cell receptors by a few peptide-MHC complexes. *Nature 375:148*.

66. Wofsy, C., D. Coombs, and B. Goldstein. 2001. Calculations show substantial serial engagement of T cell receptors. *Biophys. J. 80:606*.

67. Dombrowicz, D., S. Q. Lin, V. Flamand, A. T. Brini, B. H. Koller, and J. P. Kinet. 1998. Allergy-associated FcRβ is a molecular amplifier of IgE- and IgG-mediated in vivo responses. *Immunity 8:517*.

68. Honda, Z. I., T. Suzuki, H. Kono, M. Okada, T. Yamamoto, C. Ra, Y. Morita, and K. Yamamoto. 2000. Sequential requirements of the N-terminal palmitoylation site and SH2 domain of Src family kinases in the initiation and progression of FcεRI signaling. *Mol. Cell. Biol. 20:1759*.

69. Sheets, E. D., D. Holowka, and B. Baird. 1999. Membrane organization in immunoglobulin E receptor signaling. *Curr. Opin. Chem. Biol. 3:95*.

70. Holowka, D., and B. Baird. 2001. FcεRI as a paradigm for a lipid raft-dependent receptor in hematopoietic cells. *Semin. Immunol. 13:99*.

71. Kovarova, M., P. Tolar, R. Arudchandran, L. Draberova, J. Rivera, and P. Draber. 2001. Structure-function analysis of Lyn kinase association with lipid rafts and initiation of early signaling events after Fcε receptor I aggregation. *Mol. Cell. Biol. 21:8318*.

72. Wilson, B. S., J. R. Pfeiffer, and J. M. Oliver. 2000. Observing FcεRI signaling from the inside of the mast cell membrane. *J. Cell Biol. 149:1131*.

73. Wilson, B. S., J. R. Pfeiffer, Z. Surviladze, E. A. Gaudet, and J. M. Oliver. 2001. High resolution mapping of mast cell membranes reveals primary and secondary domains of FcεRI and LAT. *J. Cell Biol. 154:645*.

74. Ortega, E., A. Lara, I. Lee, C. Santana, A. M. Martinez, J. R. Pfeiffer, R. J. Lee, B. S. Wilson, and J. M. Oliver. 1999. Lyn dissociation from phosphorylated FcεRI subunits: A new regulatory step in the FcεRI signaling cascade revealed by studies of FcεRI dimer signaling activity. *J. Immunol. 162:176*.

75. Parravicini, V., M. Gadina, M. Kovarova, S. Odom, C. Gonzalez-Espinosa, Y. Furumoto, S. Saitoh, L. E. Samelson, J. J. O'Shea, and J. Rivera. 2002. Fyn kinase initiates complementary signals required for IgE-dependent mast cell degranulation. *Nat. Immunol. 3:741*.

76. Pribluda, V. S., C. Pribluda, and H. Metzger. 1997. Biochemical evidence that the phosphorylated tyrosines, serines, and threonines on the aggregated high affinity receptor for IgE are in the immunoreceptor tyrosine-based activation motifs. *J. Biol. Chem. 272:11185*.

Footnotes

[2] Address correspondence to Dr. Byron Goldstein, Theoretical Biology and Biophysics Group, MS K710, Theoretical Division, Los Alamos National Laboratory, Los Alamos, NM 87545. E-mail: bxg@lanl.gov

Abbreviations

ITAM, immunoreceptor tyrosine-based activation motif
MIRR, multichain immune recognition receptor
PTK, protein tyrosine kinase
RBL, rat basophilic leukemia
SH2, Src homology 2

Figure Captions

Figure 1. Model for the early events in FcεRI signaling induced by a bivalent ligand: Representation of molecular components and states. (a) The bivalent ligand shown is a covalently cross-linked IgE dimer. The tetrameric form of FcεRI, the high affinity receptor for IgE, consists of an α subunit that binds IgE, a β subunit, and a disulfide-linked dimer of γ subunits. The β and γ subunits contain ITAMs that become phosphorylated on tyrosine residues. The membrane-associated kinase Lyn can associate with the unphosphorylated or phosphorylated β subunit. The cytosolic kinase Syk associates with a doubly phosphorylated γ ITAM. On the representations of the kinases, notches indicate SH2 domains. The tandem SH2 domains of Syk are lumped together in the representation. On β, γ, and Syk, bumps represent groups of tyrosines that are lumped in the model as single targets for phosphorylation. On Syk, the model distinguishes tyrosines in the linker region, which are phosphorylated by Lyn, and those in the activation loop, which are phosphorylated by Syk. **(b)** The α subunit can be bound to ligand or unbound (2 states of α). The β subunit can be unphosphorylated or phosphorylated, with or without associated Lyn (4 states of β). The γ dimer can be unphosphorylated or phosphorylated and the phosphoryated form can be bound to Syk in any of four states of phosphorylation (6 states of γ). **(c)** There are 300 possible states for cross-linked FcεRI dimers, of which 164 contain autophosphorylated Syk. Three of these states containing active Syk are shown.

Figure 2. **The 15 reaction classes and 21 rate constants in the model.** The number of reactions contained in each class (counting forward and reverse reactions separately) is listed in parenthesis.

Figure 3. Simulated and observed kinetics of phosphorylation and other early signaling events following incubation of RBL cells with 1.6 nM IgE dimer. Curves show model predictions. Data points in (b) and (d) are from densitometric measurements of phosphorylation in a single representative experiment, plotted previously in Fig. 4 of Ref. (27). For quantitative comparison with model predictions, all data were scaled, using a common scaling factor, so that predicted and observed levels of β

phosphorylation matched at 64 min. Other scaling choices are possible and there is no obvious best choice because the factor needed to convert from optical density to receptor fraction varies from experiment to experiment and is not measured. **(a)** Predicted percentage of receptors in aggregates. **(b)** Percentage of receptors phosphorylated on β or γ ITAMs. **(c)** Predicted amount of Lyn per receptor in each of its three possible states—free, weakly associated with unphosphorylated FcεRIβ, or bound through its SH2 domain to the phosphorylated β ITAM. The total amount of available Lyn is 7% of the number of receptors. **(d)** Amount of Syk per receptor phosphorylated by Lyn (dotted line), phosphorylated by Syk (dashed line), phosphorylated by Lyn or Syk (solid line).

Figure 4. Comparison between simulated and experimental dose-response curves for receptor and Syk phosphorylation at 10 minutes as a function of initial IgE dimer concentration. The experimental data represent the results of at least 3 independent experiments in which RBL cells were exposed to the indicated concentrations of IgE dimer. Open squares show mean values and error bars show standard errors. Since the level of phosphorylation for each experiment was determined relative to the phosphorylation at 2 nM, no error bars are shown for this point. The absolute level of phosphorylation is not determined in the experiments, therefore we have scaled the experimental data so that the predicted and measured values match at 2 nM. **(a)** Percentage of receptors in aggregates. **(b)** Percentage of receptors phosphorylated on β ITAMs (dotted line), γ ITAMs (dashed line), total (solid line). **(c)** Ratio of the number of γ dimers phosphorylated to the number of β subunits phosphorylated. **(d)** Amount of Syk per receptor phosphorylated by Lyn (dotted line), phosphorylated by Syk (dashed line), phosphorylated by Lyn or Syk (solid line).

Figure 5. Dephosphorylation of FcεRI following disaggregation of receptors. Predicted (thick solid lines) and measured (filled circles) (49) fraction of receptors that remain phosphorylated after the addition of monovalent hapten to break up receptor aggregates. The thin dashed lines show the much slower dephosphorylation that results when the intrinsic dephosphorylation rate in the model, d, is set to the experimentally observed dephosphorylation rate, d_{obs}. The thin dotted lines show the increased rate of dephosphorylation when the amount of Lyn or Syk is reduced 10-fold. The thin solid

lines show the fraction of receptors remaining in dimers, which break up at a rate of 1 s^{-1} in these simulations.

Figure 6. Predicted receptor phosphorylation ratio, and fraction of Syk autophosphorylated, as a function of the number of available Syk or Lyn molecules per cell. Phosphorylation is simulated at 10 minutes following addition of 10 nM IgE dimer. **(a)** Ratio of γ to β receptor subunit phosphorylation, as a function of the Syk concentration with the amount of Lyn fixed at 2.8×10^4 per cell. **(b)** Fraction of Syk autophosphorylated, as a function of the Syk concentration. **(c)** Ratio of γ to β receptor subunit phosphorylation, as a function of the Lyn concentration with the amount of Syk fixed at 4×10^5 per cell.

Figure 7. Predicted Syk autophosphorylation as a function of the number of available Syk or Lyn molecules per cell. Phosphorylation is simulated at 10 minutes following addition of 10 nM IgE dimer. The number of autophosphorylated Syk molecules per cell (solid lines) is plotted as a function of the concentration of **(a)** Lyn and **(b)** Syk. Power law fits at low kinase concentrations (dashed lines) give exponents of 2.1 for Lyn and 2.0 for Syk.

Figure 8. Simulation of kinetic proofreading through variation of the rate constant for ligand dissociation. The values shown are obtained at steady state. The forward rate constants are fixed at $k_{+1}=10^6$ M^{-1} s^{-1} and $k_{+2}R_T=0.5$ s^{-1}, while the reverse rate constants, $k_{-1}=k_{-2}$, are set to 0.05 s^{-1} (solid lines), 0.5 s^{-1} (dashed lines), and 5 s^{-1} (dash-dot lines). The horizontal axis indicates levels of FcϵRI aggregation, given in number of receptors per cell in aggregates. **(a)** Ligand concentrations required to achieve specified levels of receptor aggregation. **(b)** Number of receptors per cell phosphorylated on β. **(c)** Number of receptors per cell phosphorylated on γ. **(d)** Number of autophosphorylated Syk molecules per cell.

Figure 9. Simulated effect of removing the high affinity interaction between Lyn and the phosphorylated β ITAM. The reported gain is the amount of phosphorylation with the β ITAM intact divided by the amount of phosphorylation in the absence of a functional β ITAM, which is modeled by setting the rate constant for β ITAM phosphorylation, $p_{L\beta}$, to zero. Gains are reported for Syk autophosphorylation (solid

line), γ phosphorylation (dashed line), and the amount of Lyn associated with aggregates (dotted line). **(a)** Gains as a function of the ligand concentration. **(b)** Gains as a function of the rate at which Lyn transphosphorylates the γ ITAM. The two parameters in the model that govern this rate are $p_{L\gamma}$ for constitutively bound Lyn and $p^*_{L\gamma}$ for Lyn bound to the β ITAM. They are varied simultaneously keeping $p^*_{L\gamma}=3p_{L\gamma}$. The arrow in panel (a) indicates the concentration used in (b), while the arrow in (b) marks the value of $p_{L\gamma}$ used in (a).
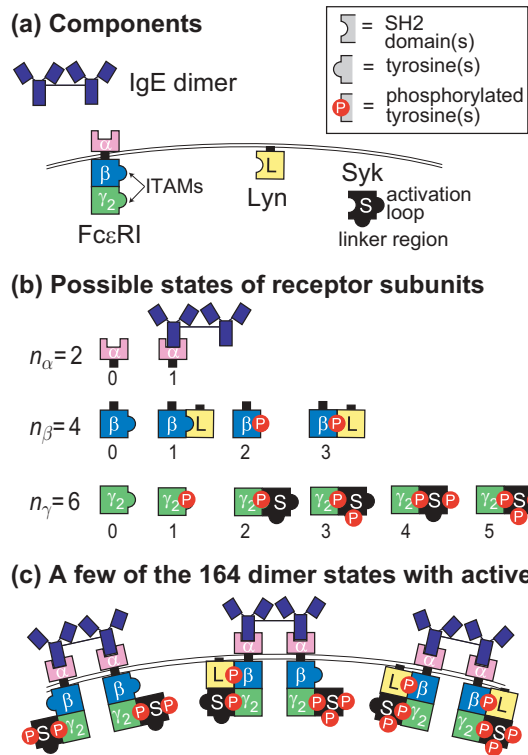
Tables

Table 1. Model Parameter Values [a]

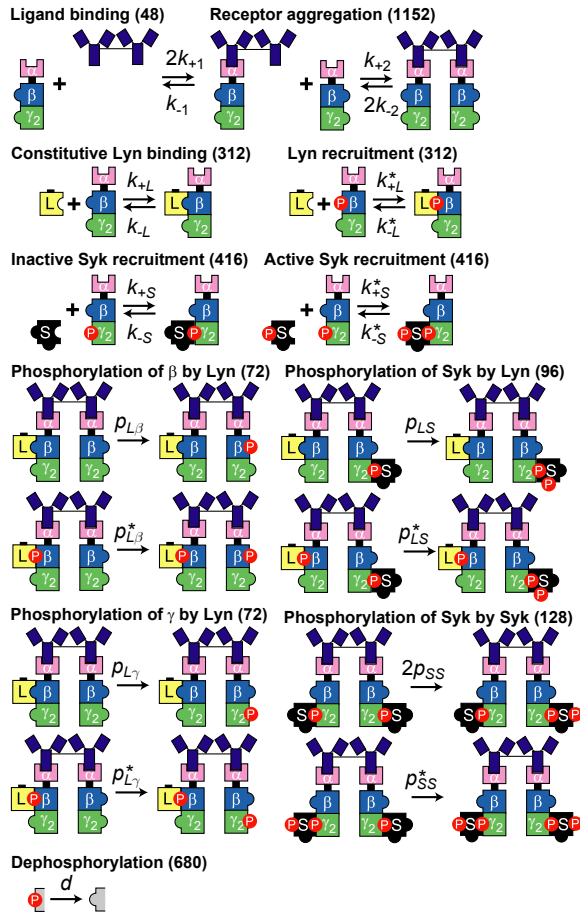| Parameter	Value	Reference
Components[b]		
Receptors, R_T	4×10^5 per cell	Current work
Lyn, L_T	2.8×10^4 per cell	Available Lyn $\sim0.07\times R_T$ (3)
Syk, S_T	4×10^5 per cell	Current work[c]
Ligand binding		
k_{+1}	1.3×10^{-10} molec^{-1} s^{-1} (8×10^4 M^{-1} s^{-1})	Estimated binding parameters for covalently cross-linked IgE dimer (3)
k_{+2}	2.5×10^{-4} molec^{-1} s^{-1}	$k_{+2}R_T$=100 s^{-1} (3)
k_{-1}, k_{-2}	0	10^{-5} s$^{-1}\sim0$ over reported time scales
Lyn association		
k_{+L}, k^*_{+L}	5×10^{-5} molec^{-1} s^{-1}	Based on estimated equilibrium constants in Ref. (3)
k_{-L}	20 s^{-1}	Based on estimated equilibrium constants in Ref. (3)
k^*_{-L}	0.12 s^{-1}	Fit to observed rate of β ITAM dephosphorylation from Ref. (49)
Syk association		
k_{+S}, k^*_{+S}	6×10^{-5} molec^{-1} s^{-1}	Based on measured equilibrium constant at 25° C for binding of Syk tandem SH2 domains (44)
k_{-S}, k^*_{-S}	0.13 s^{-1}	Fit to observed rate of γ ITAM dephosphorylation in Ref. (49)
Phosphorylation		
$p_{L\beta}$, p_{LS}	30 s^{-1}	Consistent with extensive receptor phosphorylation
$p^*_{L\beta}$, p^*_{LS}	100 s^{-1}	Moderate increase in Lyn kinase activity upon SH2 domain binding (15)
$p_{L\gamma}$	1 s^{-1}	Double phosphorylation of γ ITAM tyrosine, required to bind Syk, slower than single phosphorylation (46, 47, 76)
$p^*_{L\gamma}$	3 s^{-1}	Moderate increase in Lyn kinase activity upon SH2 domain binding (15)
p_{SS}	100 s^{-1}	Assumed same kinase activity as recruited Lyn
p^*_{SS}	200 s^{-1}	Moderate increase in Syk kinase activity upon phosphorylation of the activation loop (23)
Dephosphorylation		
d	20 s^{-1}	Fit to rates of ITAM dephosphorylation in Ref. (49)

[a]Reactions associated with these rate constants are shown in Fig. 2.
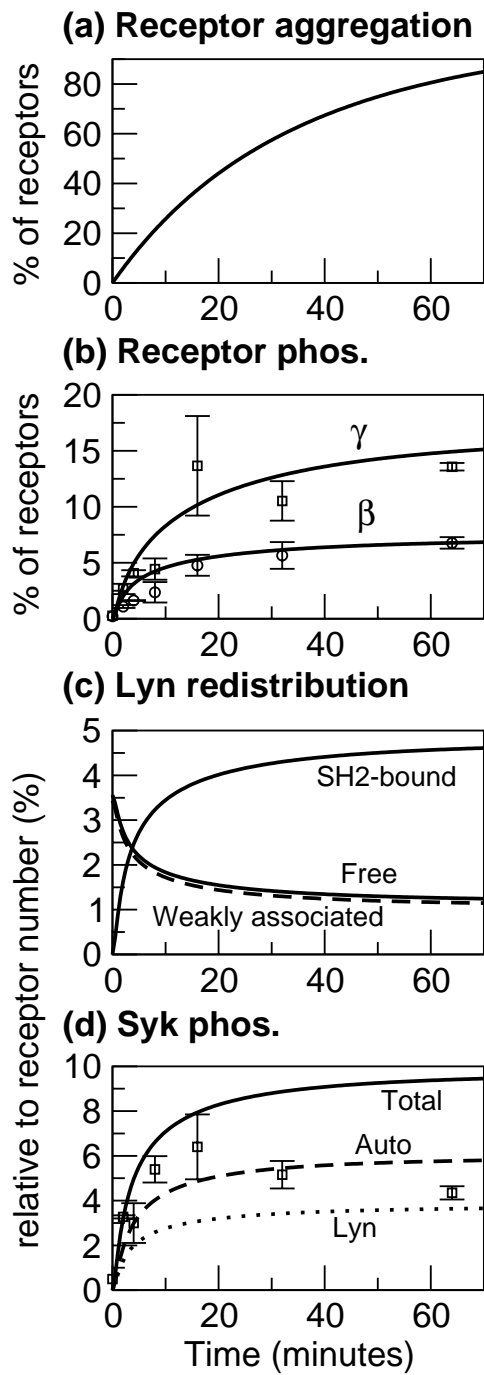[b]Cell density assumed to be 1×10^6 cells/ml. Cell volume assumed to be 1.4×10^{-9} ml.
[c]Assayed value of S_T is $3.4\pm0.4\times10^5$ per cell, which was rounded up so that $S_T=R_T$.

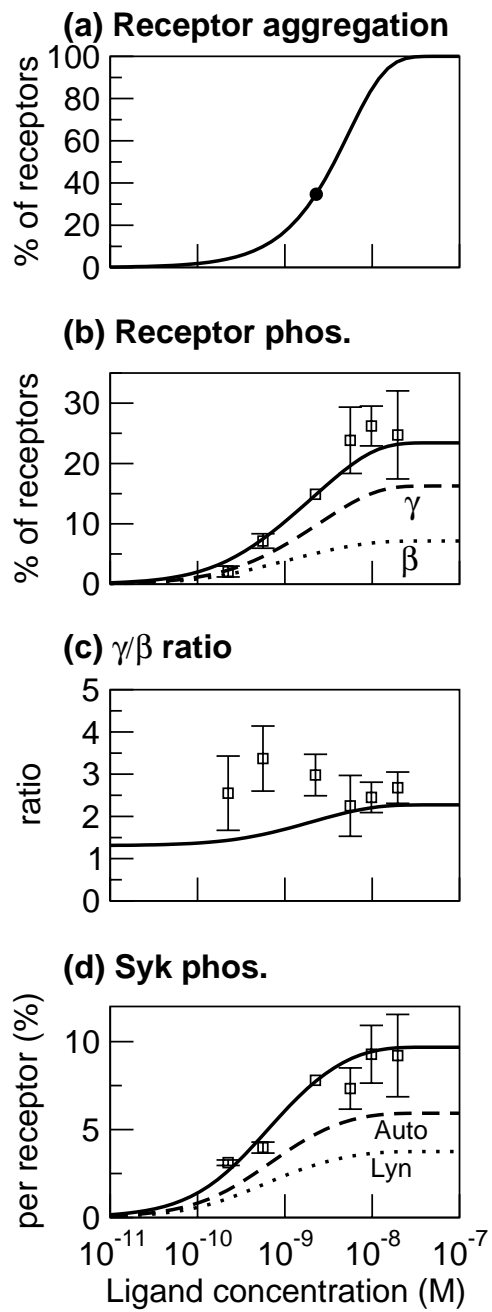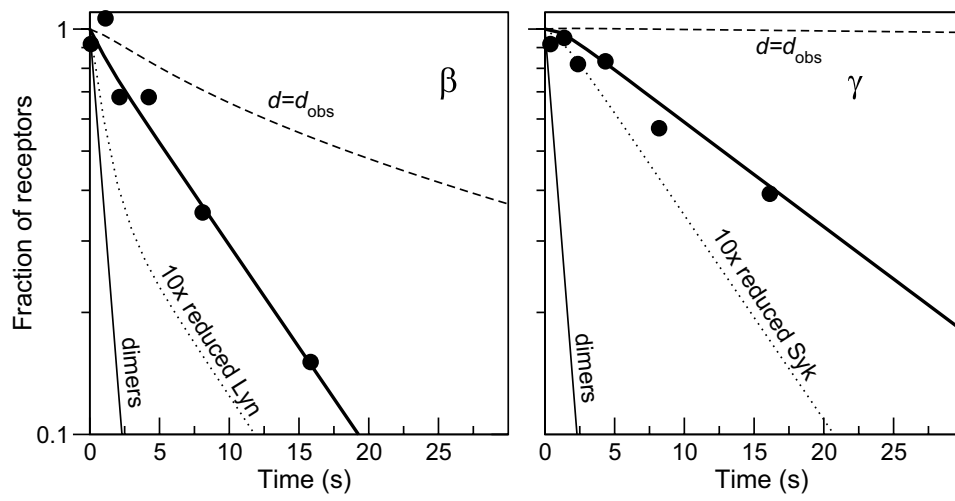**(a) Components**

IgE dimer

=	SH2 domain(s)
=	tyrosine(s)
P =	phosphorylated tyrosine(s)

FcεRI — ITAMs

Lyn

Syk — activation loop, linker region

(b) Possible states of receptor subunits

$n_\alpha = 2$

0   1

$n_\beta = 4$

β βL βP βPL
0   1   2   3

$n_\gamma = 6$

γ₂ γ₂P γ₂PS γ₂PS γ₂PSP γ₂PSP
0   1   2   3   4   5

(c) A few of the 164 dimer states with active Syk

Figure 1, Faeder *et al.*

Figure 2, Faeder *et al.*

(a) Receptor aggregation

(b) Receptor phos.

γ

β

(c) Lyn redistribution

SH2-bound

Free

Weakly associated

(d) Syk phos.

Total

Auto

Lyn

Time (minutes)

Figure 3, Faeder *et al.*

(a) Receptor aggregation
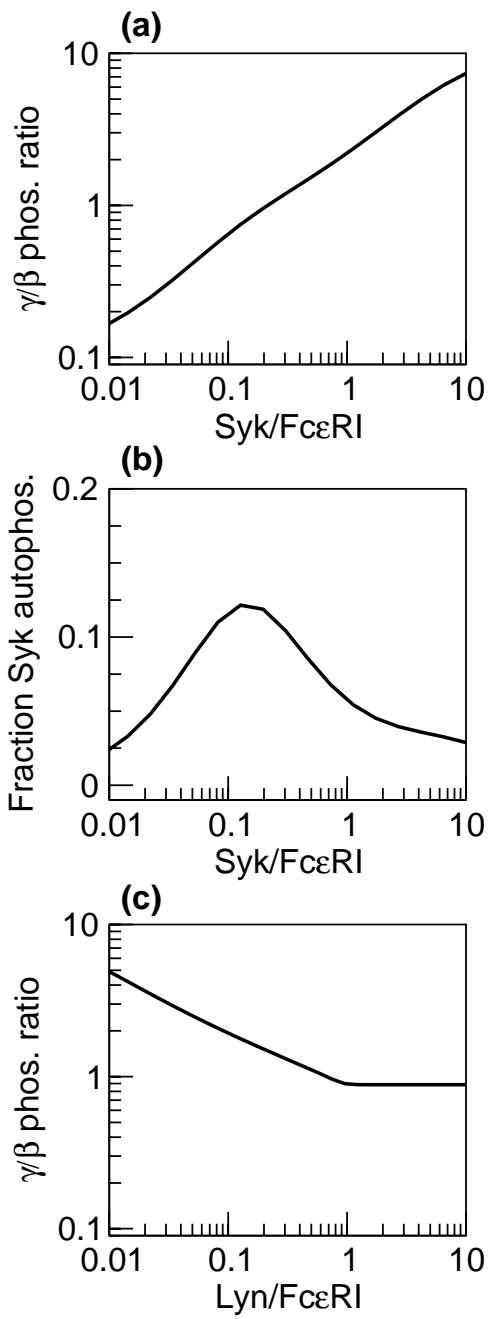
(b) Receptor phos.

(c) γ/β ratio

(d) Syk phos.

Figure 4, Faeder *et al.*

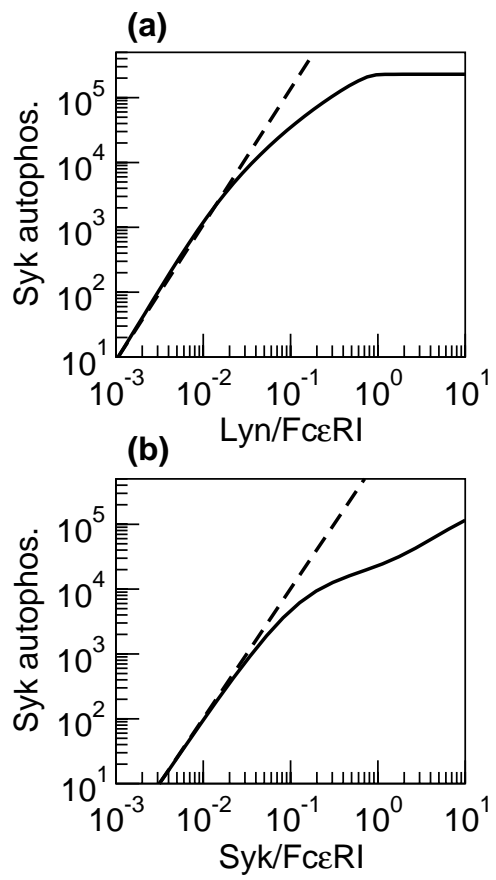**Figure 5**, Faeder *et al.*

Figure 6, Faeder *et al.*

(a)
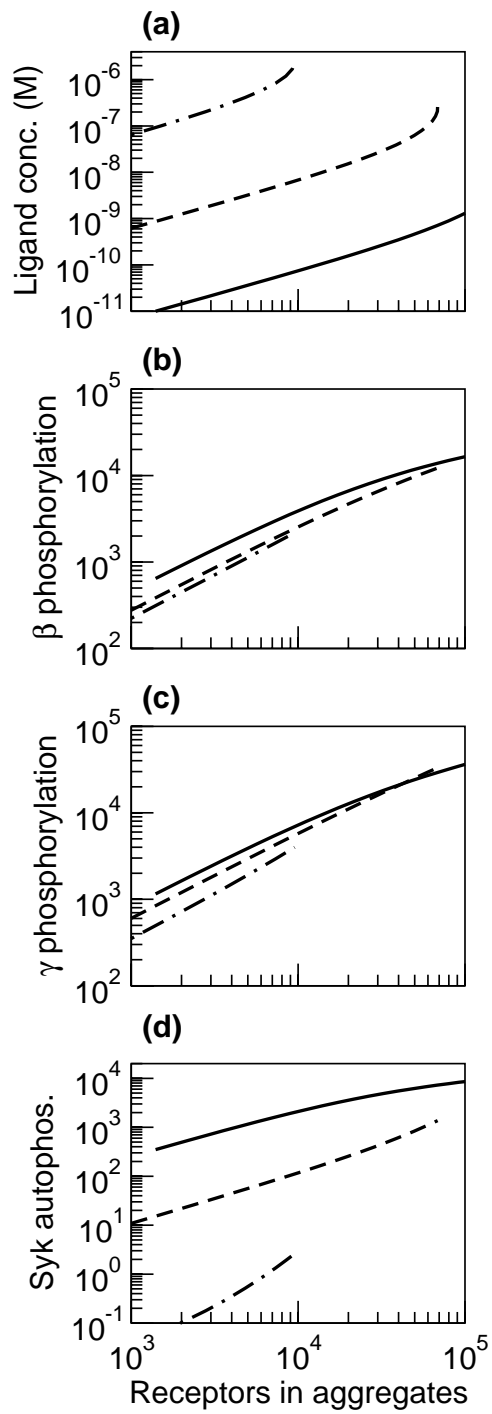
Syk autophos. vs Lyn/FcεRI
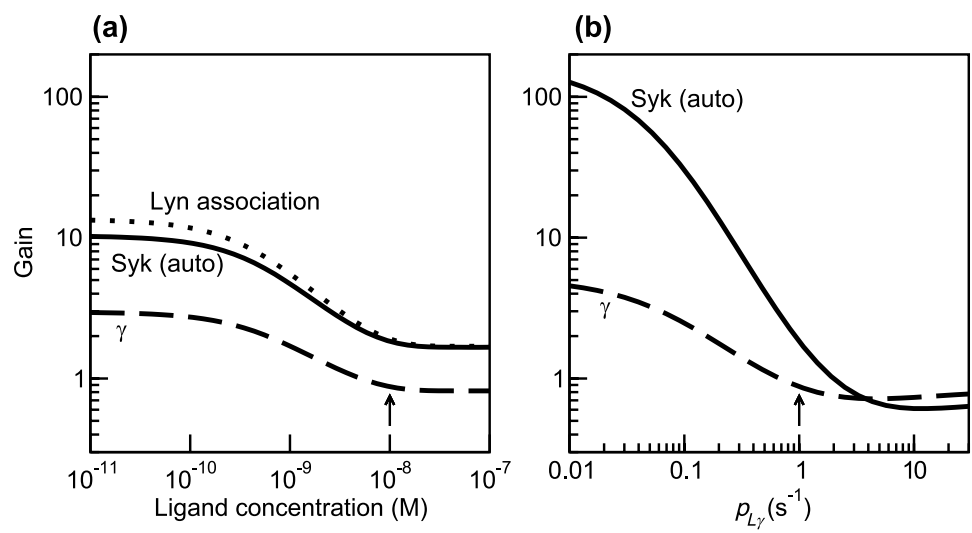
(b)

Syk autophos. vs Syk/FcεRI

Figure 7, Faeder *et al.*

Figure 8, Faeder *et al.*

Figure 9, Faeder *et al.*